Study of Transverse Flow Effects on Particle Flows and Contamination of Air Bearing Sliders: Revised

Xinjiang Shen , Mike Suk, and D.B. Bogy

ABSTRACT

For some complex slider designs the two dimensional approximation incorporated in the Reynolds equation for determining the airflow in the air bearing is not applicable due to steps in the air bearing surface. A model that incorporates some transverse flow effects is needed to better characterize the airflow between the slider and disk for some applications. In this report, such a model is derived to better predict paths of contamination particles entrained in the air bearing. The characteristics of airflow and particle flow within the air bearing are then studied. The analysis including the transverse effects reveals that the transverse velocity of the air is not negligible in the geometric transition regions of the slider. This transverse velocity has a significant effect on the flight path of particles, and therefore, on the particle contamination profile on slider surfaces. The assumption of adhesion of the particles upon impact with a surface is used as the contamination criteria, and it is viewed as the worst-case scenario.

INTRODUCTION

As required by the evolution of magnetic recording disk drive technology, the flying height of the air bearing sliders that position the read-write transducers has decreased dramatically. Currently, the minimum flying height in some products is as low as 10 nm and the track width is below 1 μm. For a particle entering the air-bearing, its possible effects include modulation of the flying height, abrasive wear and mechanical scratching of the magnetic disk surface, and thermally induced spikes in the read back signal. Flash events introduced near a MR transducer will modify the MR signal because of the dependence of MR resistance on temperature, while mechanical scratching of the magnetic disk surfaces may cause permanent data loss. These effects depend on the size and properties of the particles and their interaction with the slider and magnetic disk surfaces. Certain slider designs may reduce a particle's chance of entering the air-bearing, contacting the slider and the disk surface, and/or contaminating the slider surfaces.

The motion of a particle moving from the leading edge to the trailing edge of an air bearing is quite complicated due to the various forces acting on it. The forces are not only dependent on the particle's size, density and the air velocity and pressure fields in the air-bearing, but also on the relative velocities between the particle and the air-bearing, the particle speed and the initial entry conditions. Various expressions for determining the forces acting on a particle in unsteady gas flows have been derived by Liu and Jew (1965), Saffmann (1965) and Chen (1996).

Previously, Zhang and Bogy (1996, 1997) studied the magnitudes of the Magnus lift force, the Saffmann lift force, and gravity force. The Magnus lift force is related to

the spin of a particle in a fluid flow. If the particle's rotation speed is zero, there is no Magnus lift force. For very small particles, the gravity force is much smaller than the drag force, but for larger particles, the gravity force may not be negligible. The drag and lift forces depend on the relative velocity between the particle and the air-bearing. For airborne particles, which have very small velocities relative to the flow in the air-bearing, the Magnus lift force, Saffmann lift force and drag force could be on the same order of magnitude. Among these forces, the drag and Saffmann lift forces play important roles in large particle contamination on a slider surface.

In this paper we study some three-dimensional effects on particle contamination of slider surfaces for particles with different densities. Since the number density of the particles is small, collisions between the particles are assumed to have negligible effect and thus are neglected in the calculation. Furthermore, adhesion on first impact with the slider or disk is assumed. First, we modify the air bearing equation to include some three-dimensional flow effects. We utilize the resulting equations to calculate the forces and the motion of a particle within an air-bearing based on previous work (Zhang and Bogy, 1996, 1997, Shen and Bogy, 2002). We then choose some contemporary slider designs and show that the three-dimensional effects lead to markedly different results from the 2-dimensional flow analysis.

Transverse Flow Effects in Air-bearing Flow Analysis

In order to determine the trajectory of a particle within the air-bearing, we must first determine the spacing between the slider and disk surfaces as well as the pressure and velocity fields. For a complex slider design with etch steps, the point-to-point spacing between the slider and the disk surfaces varies abruptly in places, introducing local

three-dimensional airflow. Since the spacing is about three to five orders of magnitude less than the slider's lateral dimensions, we retain the following assumptions:

(1) The pressure gradient in the vertical direction is negligible; therefore, the pressure field calculated from the Reynolds equation is still considered to be valid.

(2) The vertical air velocity at the step regions is not negligible although it is small compared to the in-plane velocity of the air.

For different slip boundary conditions required by rarefaction effects at high Knudsen numbers, the momentum equations of the air film have different solutions. For the first order slip condition (Burgdorder, 1959; Lu, S and Bogy, D. B, 1994), we have

$$u_g\Big|_{z=0} = U + \lambda \frac{\partial u_g}{\partial z}\Big|_{z=0} \tag{1}$$

$$u_g\Big|_{z=h} = -\lambda \frac{\partial u_g}{\partial z}\Big|_{z=h} \tag{2}$$

$$v_g\Big|_{z=0} = V + \lambda \frac{\partial v_g}{\partial z}\Big|_{z=0} \tag{3}$$

$$v_g\Big|_{z=h} = -\lambda \frac{\partial v_g}{\partial z}\Big|_{z=h} \tag{4}$$

where h is the local height of the air-bearing; U, V are the speeds of the disk in the x and y directions, and λ is the mean free path of the air. Using these boundary conditions, we obtain for the non-dimensional form of velocity components of the air

$$U_g = \frac{P_0}{2\rho_g U^2}\frac{h_m}{l}\mathrm{Re}_h \frac{\partial P}{\partial X}\left(Z^2 - ZH - Kn_h H\right) + \left(1 - \frac{Kn_h + Z}{2Kn_h + H}\right) \tag{5}$$

$$V_g = \frac{P_0}{2\rho_g U^2}\frac{h_m}{l}\mathrm{Re}_h \frac{\partial P}{\partial Y}\left(Z^2 - ZH - Kn_h H\right) + \frac{V}{U}\left(1 - \frac{Kn_h + Z}{2Kn_h + H}\right) \tag{6}$$

where P is the dimensionless pressure, or pressure divided by the ambient pressure P_0; $H = \frac{h}{h_m}$ is a non-dimensional spacing of the air-bearing; $Kn_h = \frac{\lambda}{h_m}$ is the Knudsen number defined in terms of the minimum spacing height h_m. Since we continue to assume that the pressure gradient in the z direction is negligible, the pressure field of the air-bearing, P, can still be obtained from the Reynolds equation

$$\sigma \frac{\partial PH}{\partial T} = \frac{\partial}{\partial X}\left(QPH^3 \frac{\partial P}{\partial X} - \Lambda_x PH \right) + \frac{\partial}{\partial Y}\left(QPH^3 \frac{\partial P}{\partial Y} - \Lambda_y PH \right), \tag{7}$$

where $\sigma = \frac{12\mu_g \hat{\Omega} l^2}{p_0 h_m^2}$ is the squeeze number; $Q = 1 + 6a\frac{Kn_h}{PH}$ is the flow factor for the first order slip model; $a = \frac{2-\alpha}{\alpha}$ and α is the accommodation factor; Λ_x and Λ_y are the bearing numbers $\Lambda_x = \frac{6\mu_g U l}{p_0 h_m^2}$ and $\Lambda_y = \frac{6\mu_g V l}{p_0 h_m^2}$.

For the transverse velocity of the air, w, the boundary conditions are

$$w\big|_{z=0} = 0 \tag{8}$$

$$w\big|_{z=H} = 0 \tag{9}$$

Let $w = W(Z)(H - Z)U$, and substitute it into the continuity equation to obtain

$$\frac{\partial U_g}{\partial X} + \frac{\partial V_g}{\partial X} - \frac{l}{h_m}\frac{\partial [W(H-Z)]}{\partial Z} = 0 \tag{10}$$

By substituting U_g, V_g from Eqs. (5) and (6) into Eq. (10), one may integrate the result to obtain an analytical solution of the transverse velocity of the air in the air-bearing.

Particle Kinetics Equations

The governing equations for a particle moving in air can be written as

$$\frac{d\vec{x}}{dt} = \vec{v} \tag{11}$$

$$m\frac{d\vec{v}}{dt} = \vec{f} \tag{12}$$

where $\vec{x}$ and $\vec{v}$ are the position and velocity vectors of the particle, respectively; m represents the mass of the particle; $\vec{f}$ includes the forces of drag, Saffmann lift, Magnus lift and gravity acting on the particle. The electrostatic and molecular forces between particles and slider surfaces are neglected. The details of the forces are thoroughly studied by Zhang and Bogy (1997), and so they are only briefly outlined here:

(1) Drag force

For a rigid spherical particle moving in an airflow, the drag force can be expressed as

$$\vec{f}_d = \frac{\pi}{8} C_d C_w \rho_g d^2 \left\| \vec{u}_a - \vec{u}_p \right\| \left(\vec{u}_a - \vec{u}_p \right) \tag{13}$$

where C_d is the drag coefficient; C_w is the coefficient of the wall effects which tends to unity when the particle is far enough away from the wall; d is the diameter of the sphere; ρ_g is the density of the air; $\vec{u}_a$ and $\vec{u}_p$ are the velocity of the air and sphere, respectively. The details of the drag coefficient C_d and the wall effect coefficient C_w are explained by Zhang and Bogy (1997).

(2) Saffmann lift force

The lift force acting on a spherical particle in a linear shear flow can be expressed as

$$f_{SL} = \frac{9}{\pi} J \mu R^2 \Delta U \left(\frac{\rho_g G}{\mu} \right)^{1/2} \tag{14}$$

where μ is the viscosity of the air; ΔU is the velocity of the sphere relative to the airflow, which is given by $\Delta U = \frac{\left(\vec{u}_p - \vec{u}_a\right)\cdot\vec{u}_a}{\left\|\vec{u}_a\right\|}$; G is the magnitude of the airflow shear rate calculated by $G = \frac{\vec{u}_a \cdot \frac{\partial \vec{u}_a}{\partial z}}{\left\|\vec{u}_a\right\|}$; J is expressed by Cox and Hsu (1977) as $J = \frac{\pi^2}{16}\left(\frac{1}{\varepsilon} + \frac{11}{6} l_w^*\right)$. For a sphere far away from the wall J converges to the Saffmann's value of 2.255. When the sphere is close to the wall J depends on the ratio, $\varepsilon = \frac{\left(\mathrm{Re}_G\right)^{1/2}}{\mathrm{Re}_S}$, and a non-dimensional distance $l_w^* = \left(\rho_g G/\mu\right)^{1/2} l_w$ in which l_w is the distance between the sphere and wall. Here $\mathrm{Re}_s = \Delta U R \rho_g / \mu$ and $\mathrm{Re}_G = GR^2\rho_g/\mu$.

(3) Magnus lift force

The spinning of the particle and the air shear results in Magnus lift, which is expressed as

$$f_m = \frac{\pi}{8}\rho_g d^3 \left\{\left[\vec{\omega}\times\left(\vec{u}_p - \vec{u}_g\right)\right]\cdot\vec{e}_z + \frac{1}{2}\frac{\partial \vec{u}_g}{\partial z}\cdot\left(\vec{u}_p - \vec{u}_g\right)\right\} \tag{15}$$

where $\vec{\omega}$ is the angular velocity vector of the particle; $\vec{e}_z$ is the unit vector in the z direction. The Magnus lift force is usually negligible for submicron particles compared to the Saffmann lift force as shown here.

(4) Gravity force

The gravity force is given as

$$\vec{f} = \frac{4}{3}\pi R^3 \left(\rho_g - \rho_p\right)\vec{g} \tag{16}$$

where $\vec{g}$ is the acceleration due to gravity. The buoyancy force is also included in the calculation although it is negligible compared to the gravity force. Substituting the various force equations into the governing equations of the particle and rearranging the terms in non-dimensional forms, we obtain

$$\frac{dX_p}{dT} = R_l U_p \tag{17}$$

$$\frac{dY_p}{dT} = R_l V_p \tag{18}$$

$$\frac{dZ_p}{dT} = R_h W_p \tag{19}$$

$$\frac{dU_p}{dT} = \frac{3}{4} R_h \frac{\rho_g}{\rho_p} \frac{C_d C_{wx}}{D} \bar{U}\left(U_g - U_p\right) \tag{20}$$

$$\frac{dV_p}{dT} = \frac{3}{4} R_h \frac{\rho_g}{\rho_p} \frac{C_d C_{wy}}{D} \bar{U}\left(V_g - V_p\right) \tag{21}$$

$$\begin{aligned}\frac{dW_p}{dT} &= \frac{3}{4} R_h \frac{\rho_g}{\rho_p} \frac{C_d C_{wz}}{D} \bar{U}\left(W_g - W_p\right) + \frac{27}{32}\left(\frac{1}{\varepsilon} + \frac{11}{6} l_w^*\right) R_h \,\mathrm{Re}_h^{-1/2} \frac{\rho_g}{\rho_p} \frac{\hat{U}}{D} k^{1/2} \\ &+ R_h \left(\frac{\rho_g}{\rho_p} - 1\right) \frac{h_m}{\hat{U}^2} g_z + \frac{3}{4} R_h \frac{\rho_g}{\rho_p}\left(\frac{\Omega_{py}}{R_h} - 1/2 \frac{\partial U_g}{\partial z}\right)\left(U_g - U_p\right) \\ &- \frac{3}{4} R_h \frac{\rho_g}{\rho_p}\left(\frac{\Omega_{px}}{R_h} + 1/2 \frac{\partial V_g}{\partial z}\right)\left(V_g - V_p\right)\end{aligned} \tag{22}$$

$$\frac{d\Omega_{py}}{dT} = -60 \frac{R_h^2}{\mathrm{Re}_h D^2} \frac{\rho_g}{\rho_p}\left(\frac{\Omega_{py}}{R_h} - 1/2 \frac{\partial U_g}{\partial z}\right) \tag{23}$$

$$\frac{d\Omega_{px}}{dT} = -60 \frac{R_h^2}{\mathrm{Re}_h D^2} \frac{\rho_g}{\rho_p}\left(\frac{\Omega_{px}}{R_h} + 1/2 \frac{\partial V_g}{\partial z}\right) \tag{24}$$

where $X = x/l$, $Y = y/l$ and $Z = z/h_m$ are non-dimensional position variables; l is the length of the slider and h_m is the initially given height of the air-bearing at the trailing edge; $U = \frac{u}{\hat{U}}, V = \frac{v}{\hat{U}}$ and $W = \frac{w}{\hat{U}}$ are non-dimensional velocity components of the particle; T is the dimensionless time $T = \hat{\Omega} t$, and $\hat{\Omega}$ is the rotation speed of the disk. $\overline{U} = \sqrt{(U_g - U_p)^2 + (V_g - V_p)^2}$, and $\hat{U} = \Delta U / \hat{U}$, where ΔU is the velocity of the sphere relative to the airflow, and $\hat{U}$ is the disk velocity. U_g, V_g and U_p, V_p denote the velocity components in the x and y directions of the air and the sphere, respectively. D is the non-dimensional diameter of the particle, which is $D = d/h_m$. R_l and R_h are non-dimensional numbers, defined as $R_l = \frac{\hat{U}}{\hat{\Omega} l}$, $R_h = \frac{\hat{U}}{\hat{\Omega} h_m}$. In Eqs. (23) and (24), $\mathrm{Re}_h = \frac{\hat{U} h_m}{\nu}$ is the Reynolds number, $\Omega_{px} = \frac{\omega_{px}}{\hat{\Omega}}$, and $\Omega_{py} = \frac{\omega_{py}}{\hat{\Omega}}$ where ω_{px}, ω_{py} are the angular velocities of the sphere with respect to the x and y axes.

For particle flow analysis, the number of particles and their sizes can be determined from experiments. The particles are first assumed to be uniformly distributed above the disk surface with velocities close to the air-bearing's velocity where the particles are located, which are calculated by Eqs. (5) and (6). The particle's initial vertical velocity is assumed to be negligible.

Numerical Results and Discussions

In this section, the three-dimensional airflow effects on particle trajectories and contamination are studied. A representative modern negative pressure slider is chosen for this study (Fig. 1.) The flying height of the slider is 26 nm, with a pitch angle of

76 μrad and a roll angle of -1.8 μrad at the radius of 14.5mm. The pressure profile shown in Fig. 2 is obtained without 3-d effects by solving the Reynolds equation for the air-bearing of the slider using the CML code Quick 4.

To study particle flow in the air-bearing, we first calculated the spacing function between the slider and the disk. The slider-disk spacing map is shown in Fig. 3, where it can be observed that particles may enter the recessed region of the air-bearing through the leading edge of the slider. Next, the streamlines at different levels of the slider/disk spacing were calculated for heights above the disk of 1%, 50% and 99% of the spacing as shown in Figs. 4(a)-(c) taking into account the effects of transverse flow. It is shown that the airflow close to the disk is mainly determined by the disk velocity and skew angle, while close to the slider surface the streamlines are mainly determined by the slip boundary conditions of the air. The air streamline pattern at 50% follows the shape of the air-bearing. Previously, the vertical velocity of the air was assumed to be zero for the air-bearing, according to 2-D air bearing theory. However, due to the complex geometry of the slider, there is a pressure step change between the leading pad and the recess region. The pressure gradient and geometry (as shown in Figs. 5) cause the air to move vertically up along the wall according to the modified theory with transverse effects, as shown in Fig. 6. Evidently, in the recess and ABS regions, the transverse airflow is still negligible since the pressure gradient is small and the air can be treated as flow between two parallel planes. In the transition zone (x/xl=0.08 in Fig. 6), the maximum transverse air velocity is 0.5U, where U is the disk velocity where the slider is located. This is about half of the 2-D velocity and thus, it can not be neglected. The drag force in the

transverse direction acting on a particle due to this airflow is also not negligible in these regions.

By applying the transverse flow force component to the particle flow analysis as stated in the previous section, we can make a comparison of particle trajectories between the air bearing solutions without and with the transverse effects as shown in Fig. 7. It is shown that an airborne particle's trajectory predicted by the purely 2-D airflow analysis is almost parallel to the disk surface since the lift forces acting on it are so small and there is almost no drag force. The drag force acting on the particle in the purely 2-D model is only on the order of -1E-14 micro Newton, while the drag force acting on this particle taking into account the transverse effect model is -1E-10 micro Newton before the leading edge and 1E-7 micro Newton between the leading pad and recess region, which is about 4-7 orders of magnitude higher due to the transverse air flow in the different regions. Also the lift force acting on the particle in Figure 7 is between 1E-11 and 1E-9 micro Newton. To further understand the transverse flow effects, a comparison of drag force and Saffmann lift force at various locations was carried out for the two models. The locations used for comparison are illustrated in Fig. 8. The results are also given in Table 1. It is shown that the drag force contributes significantly in the transverse flow model (usually 2 orders higher than in the purely 2-D modeling), with little contribution from the Saffmann lift force. Due to the drag force effect, the transverse flow analysis predicts that the particle's path is modified at the places of abrupt change in the slider-disk spacing. In this case, the drag force is the main cause of the vertical motion of the particle. Figure 9 shows different trajectories for particles starting from different locations. Here we see that all particles are affected by the transverse airflow in the transition regions, and the drag

force acting on the particles close to the disk surface is much smaller according to the calculations.

Applying the flow with and without transverse effects to the particle contamination analysis, we can compare the calculated contamination profiles (Fig. 10), which shows a large difference between the two results. The particle contamination profile obtained by the purely 2-D analysis has many particles on the leading pad and there are no particles attached to and after the transition regions of the air-bearing surface. By contrast, few particles are observed on the leading pad and a greater number of particles are observed in the transition region between the leading pad and the recess region according to the airflow analysis with transverse effects.

Figure 11 shows the effect of particle density. Particles of extremely low density (0.1 g/cm^3) cannot approach the slider and contaminate it since the particle's Stokes number is extremely small. For a high density particle (36 g/cm^3), the particle's path is highly influenced by its inertia so it is less prone to move upwards to the slider surface. Therefore it travels farther through the air bearing without impacting the slider. The density of the particles used in the analysis was 4.25 g/cm^3, which is the composite density of the commonly used slider material (Al_2O_3). Particles of this density can easily contaminate the transition regions between the leading pad and recess regions thereby explaining the particle contamination profile difference shown in Fig. 11. Heavy particles are more prone to collect in the recess regions than in the transition regions, as shown in Fig. 12. Figure 13 shows the number of particles contaminating the inner leading pad, outer leading pad and trailing pad as a function of density. It is shown that with the increase in the mass density of the particle the

number of particles on the trailing pad increases while the number of the particles on the leading pads decreases. However, for the extremely low density particles, the number of particles on all of the regions increases with density since the flow of particles is dominated by the particles' Stokes number (Nguyen and Fletcher, 1999).

Figures 14 and 15 show a comparison of the numerical simulation of a particle contamination profile with experiments for a particular slider design. One can see in both figures that many particles strike the front edge of the rails. These are large particles coming from the entrance. In Figure 15, mostly particles of 100 nm are deposited in this region. There are also many small particles that pass through the spacing between the slider and disk surfaces (< 50nm spacing). For these particles, we used 30 nm in the simulation. The numerical simulation is seen to agree quite well with the experiment.

SUMMARY AND CONCLUSIONS

From the multi-particle flow analyses in the air bearing we observe that the analysis with transverse flow effects predicts results that are quite different from those predicted by the purely 2-dimensional air bearing theory. We observe that with the transverse effects the particles are more likely to contaminate the transition regions on the rail surfaces between the leading pad and recessed regions, a result not predicted by the 2-D flow analysis. It is also found that the heavier particles travel a longer distance under the slider before contacting the slider surface due to their inertia, while very light particles rarely contact the slider since the stokes number of the particles is very small. Therefore, heavier particles are more likely to collect on the trailing pad

of the slider surface than the lighter particles. By improving the airflow of the slider using different ABS designs, it may be possible to reduce the contamination problem.

Acknowledgements

The authors thank Jose Castillo (Iomega Inc, Utah) for many fruitful discussions and suggestions. We also thank him for providing experimental data on particle contamination for the particular slider we simulated.

References

[1] Xinjiang Shen and David B. Bogy, 2002**, "**Particle Flow and Contamination in Slider Air Bearings for Hard Disk Drives", CML Technical Report 2002-01.

[2] Burgdorder, A., 1959, "The Influence of the Molecular Mean Free Path on the Performance of Hydrodynamics Gas Lubricated Bearing", ASME Journal of Basic Engineering, **81**(1), pp.94-100.

[3] Cha, E. T. and Bogy, D. B., 1995, "A Numerical Scheme for Static and Dynamic Simulation of Sub ambient Pressure Shaped Rail Sliders", ASME Journal of Tribology, **117**, pp.36-46.

[4] Chen, X., 1996, "The Drag Force acting on a Spherical Non-evaporating or evaporating particle immersed into a rarefied plasma flow", Journal of Physics D: Applied Physics, **29**, pp. 995-1005.

[5] Clift, R. Grace, J. R. and Weber, M. E., 1978, Bubbles, Drops, and Particles, Academic Press.

[6] Cox, R. G. and Hsu, S. K., 1977, "The Lateral Migration of Solid Particles in A Laminar Flow Near a Plane", International Journal of Multiphase Flow, **3**, pp.201-222.

[7] Fukui, S. and Kaneko, R., 1988, "Analysis of Ultra-thin Gas Film Lubrication Based on Linearized Boltzmann Equation: First report-Derivation of a Generalized Lubrication Equation Including Thermal Creep Flow", ASME Journal of Tribology, **110**, pp.253-261.

[8] Fukui, S. and Kaneko, R., 1990, "A Database for Interpolation of Poiseuille Flow Rates for High Knudsen Number Lubrication Problems", ASME Journal of Tribology, **112**, pp. 78-83.

[9] Hsia, Y. T., Domoto, G. A., 1983, "An Experimental Investigation of Molecular Rarefaction Effects in Gas Lubricated Bearings at Ultra –low Clearnce", ASME Journal of Tribology, **105**(1), pp. 120-130.

[10] Liu, V. C., Pang, S. C. and Jew, H., 1965, "Sphere Grad in Flows of Almost -Free Molecules", Physics of Fluids, **8**(5), pp. 788-796.

[11] Lu, S. and Bogy, D. B., 1994, "A Multi-Grid Control Volume Method for the Simulation of Arbitrarily Shaped Slider Air-bearing with Multiple Recess levels", CML Technical Report, No. 94-016, Department of Mechanical Engineering, University of California at Berkeley.

[12] Maxey, M. R., 1993, "The Equation of Motion for a Small Rigid Sphere in a Nonuniform of Unsteay Flows", Gas-Sold Flows, ASME FED **166**, pp. 57-62.

[13] Mclaughlin, J. B., 1993, " The Lift on a Small Shpere in Wall-bounded Linear Shear Flows", Journal of Fluid Mechanics, **246**, pp. 249-265.

[14] Millikan, R. A., 1923, "The General Law of Fall of A Small Spherical Body through A Gas, and Its Bearing Upon the Nature of Molecular Reflection from Surfaces", Physics Review, **22**(1), pp. 1-23.

[15] Rubinov, S. I. And Keller, J. B., 1961, " The Transverse Force on A Sphere Moving in A Viscous Fluid", Journal of Fluid Mechanics, **11** (3), pp. 447-459.

[16] Saffman, P. G., 1965, "The lift on a Small Sphere in A Slow Shear Flow", Journal of Fluid Mechanics, **22**, pp. 385-400.

[17] Schaaf, A. L. and Chambre, P. L., 1961, Flow of Rarefied Gases, Princeton University Press, Princeton, US.

[18] Zhang, S., 1997, Numerical Investigation of Particle Contamination and Thermal Effects in a Slider Disk Interface, Doctoral Dissertation, Department of Mechanical Engineering, University of California, Berkeley.

[19] Zhang, S. and Bogy, D. B., 1996, "Effects of Lift on the Motion of Particles in the Recessed Regions of a Slider", CML Technical Report, No. 96-016, Department of Mechanical Engineering, University of California at Berkeley.

[20] Nguyen, A. V. and Fletcher, C.A. J., 1999, "Particle interaction with the wall surface in two-phase gas-solid particle flow", International Journal of Multiphase Flow, **25**, pp.139-154.

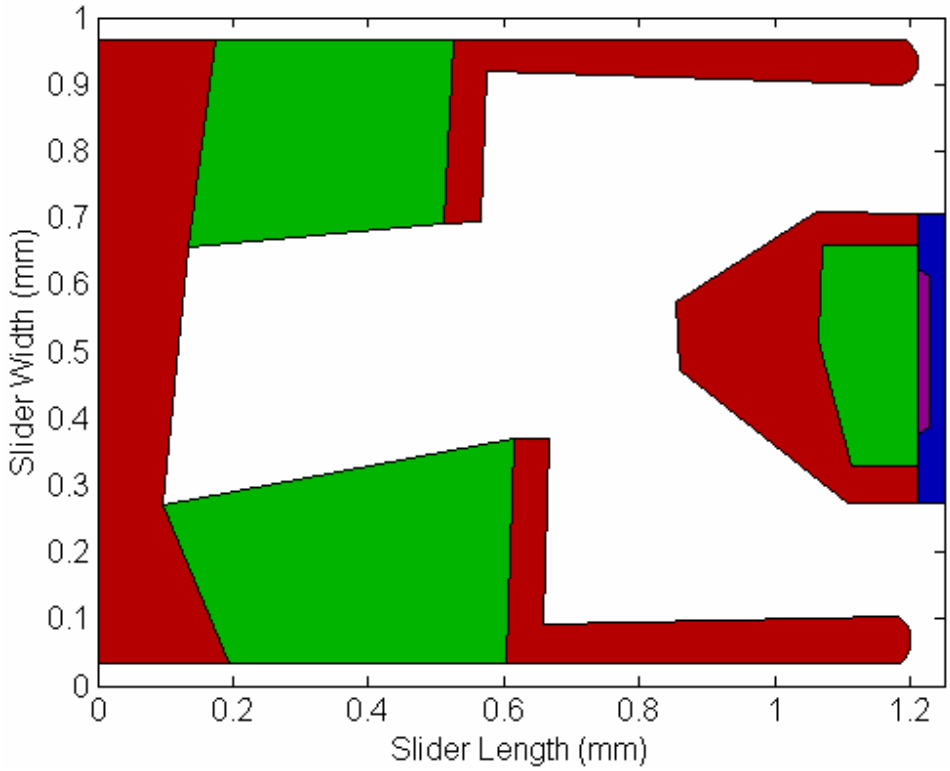

Figure 1, 2-D rails of one example slider.

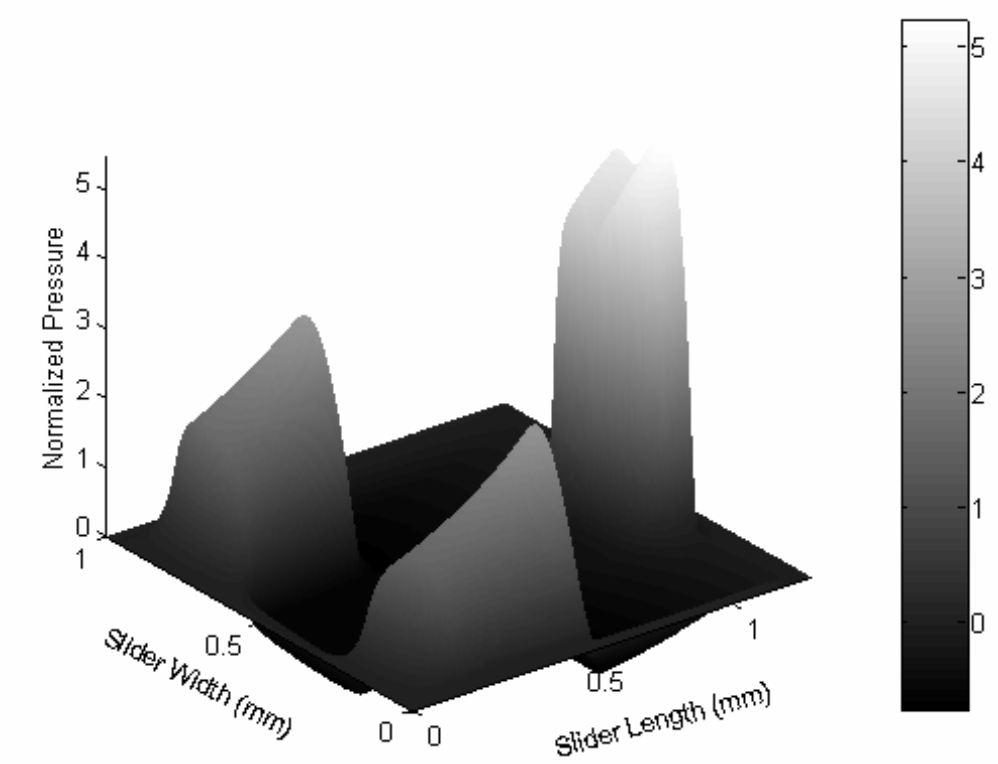

Figure 2, Pressure profile of the air-bearing for the slider.

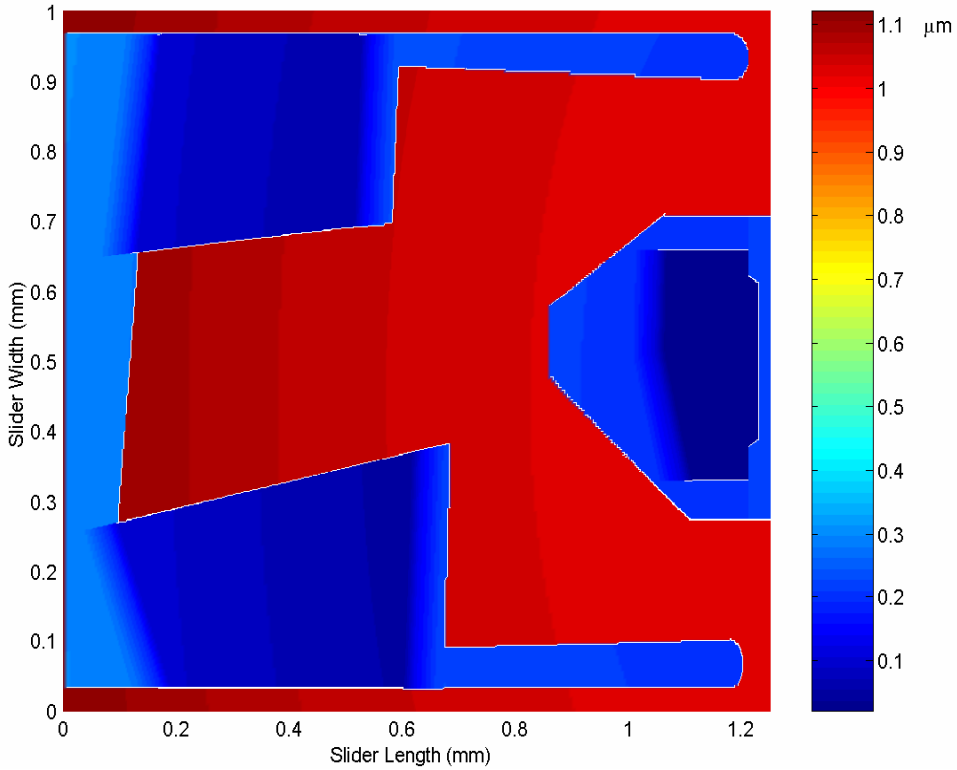

Figure 3, Spacing between the slider and disk surfaces.

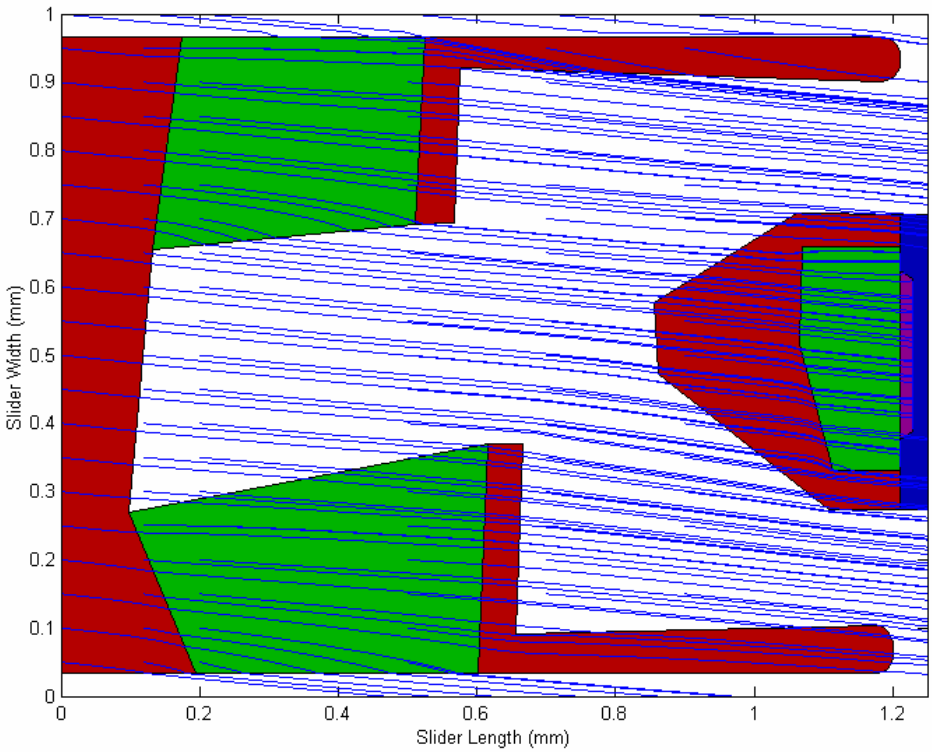

Figure 4 (a), Air streamlines at heights of 1% of the slider spacing above the disk.

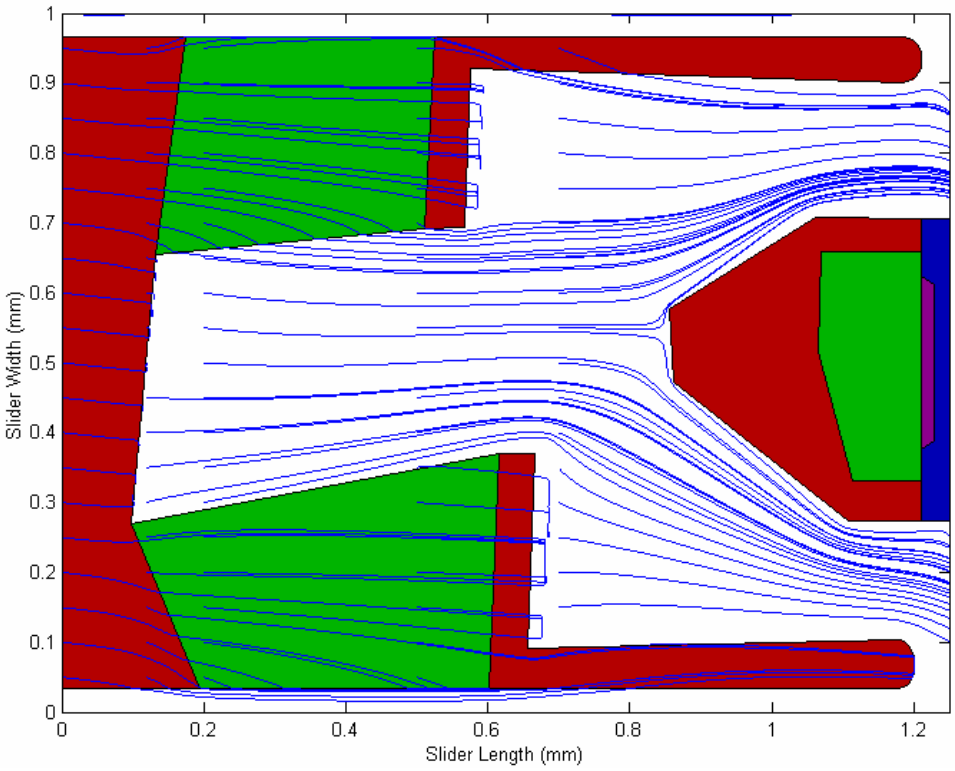

Figure 4 (b), Air streamlines at heights of 50% of the slider spacing above the disk.

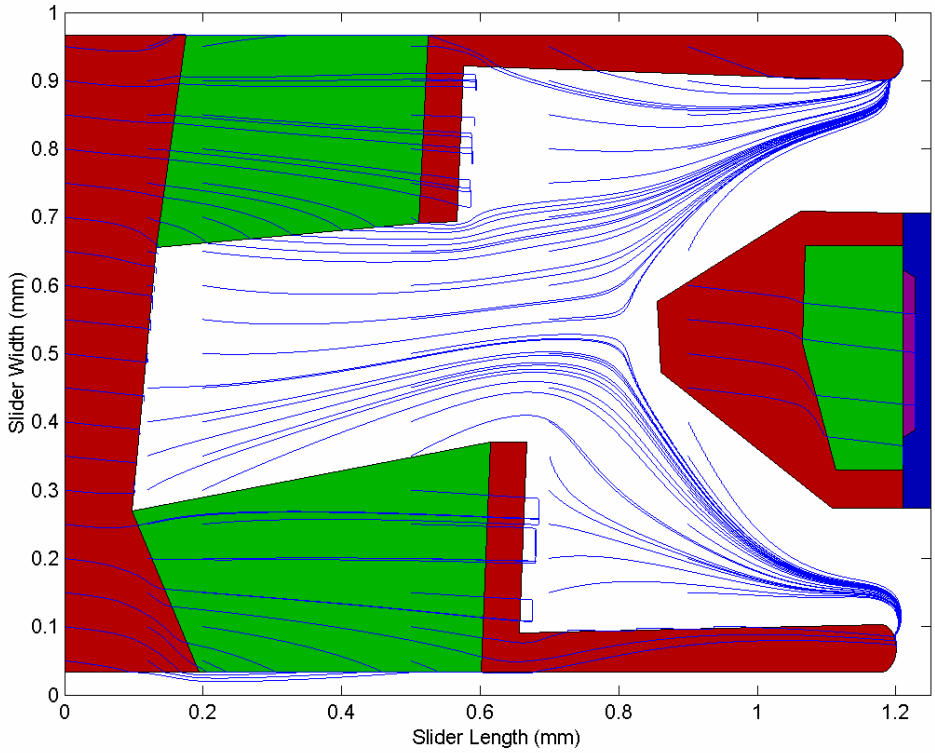

Figure 4 (c), Air streamlines at heights of 99% of the slider spacing above the disk.

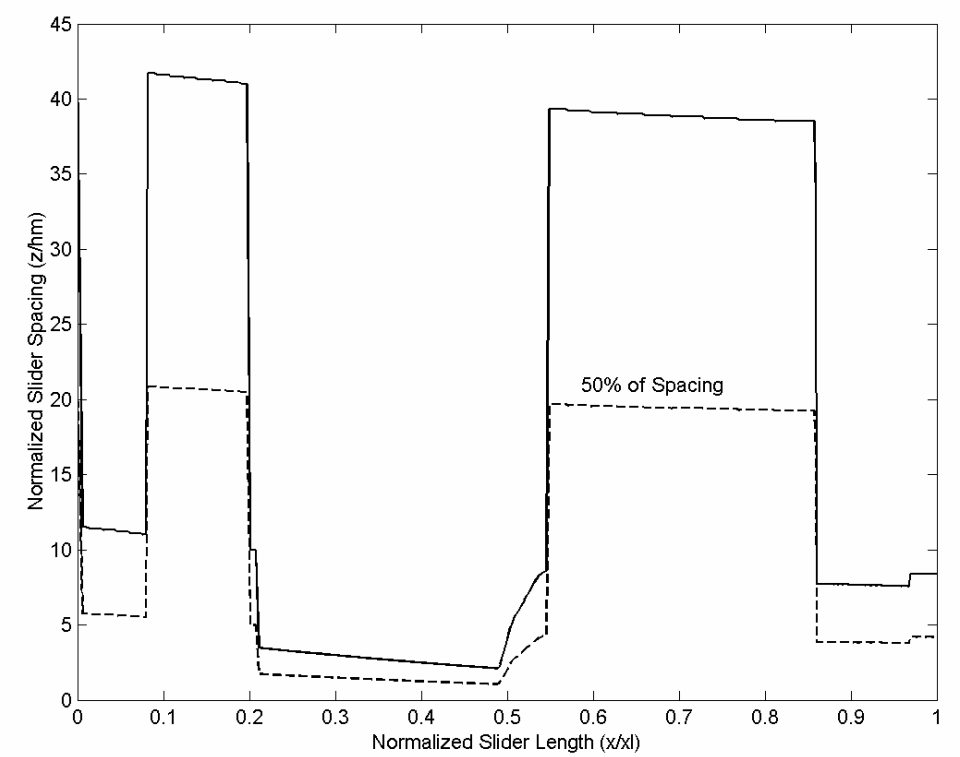

Figure 5, Spacing between the slider and disk surfaces at y=0.3 mm.

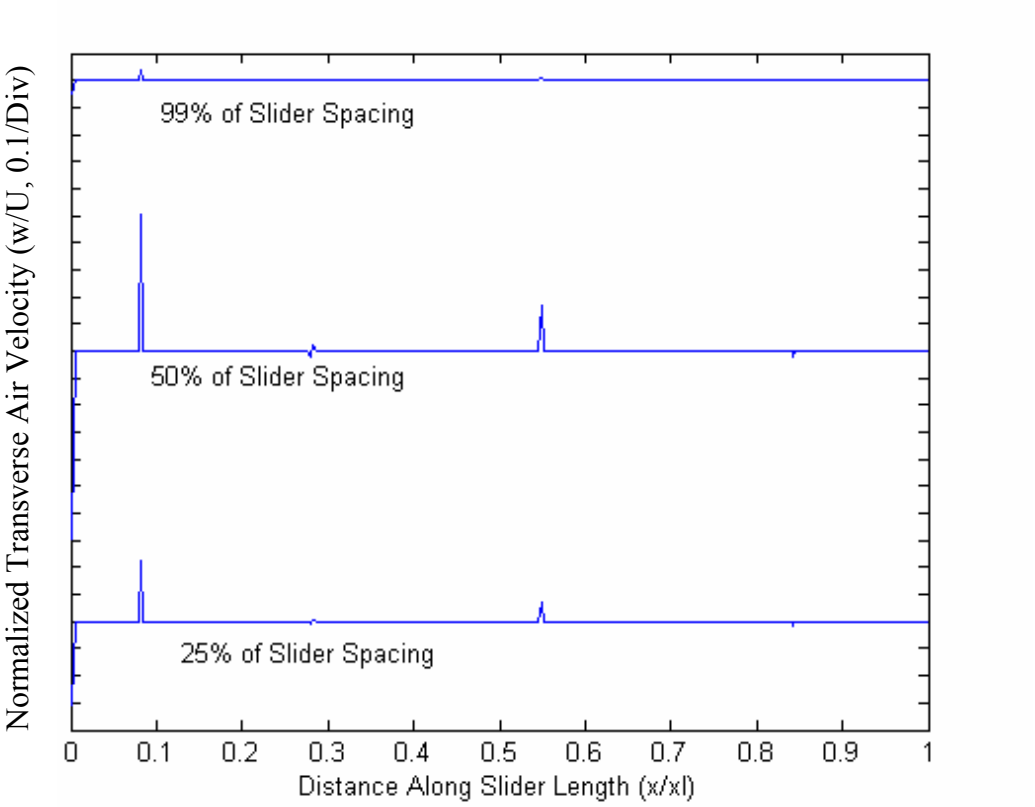

Figure 6, Air vertical velocity in the air-bearing at y=0.3 mm.

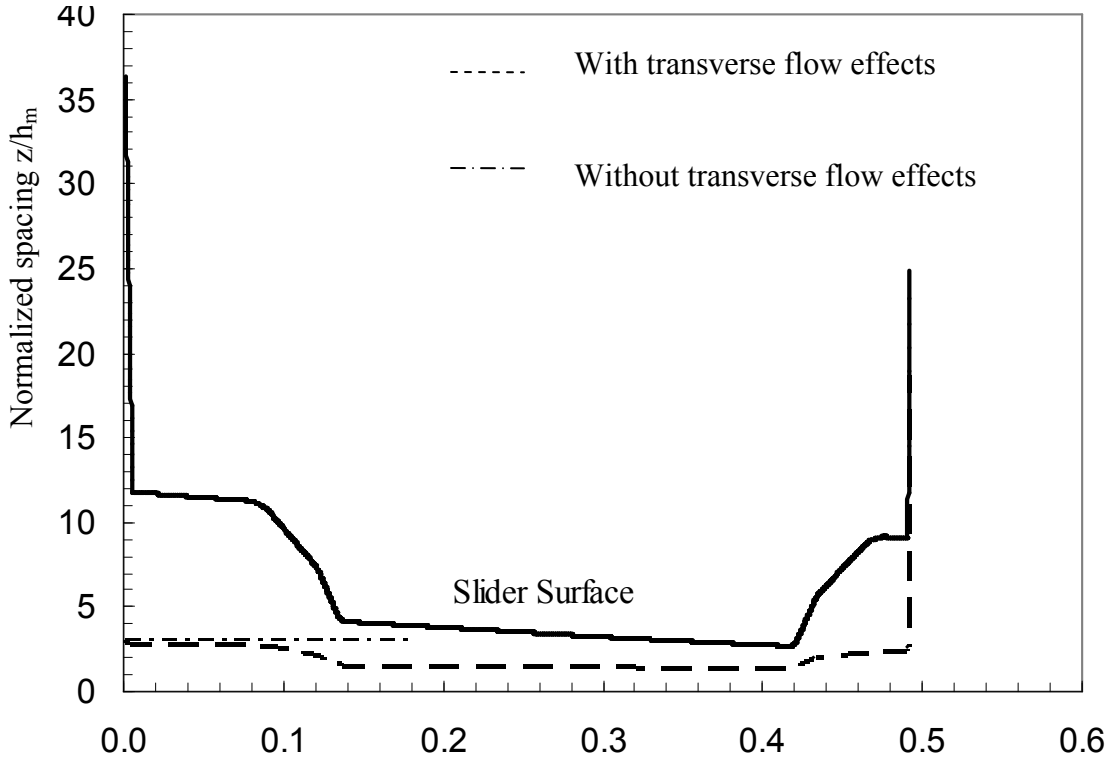

Figure 7, Comparison between particle trajectories.

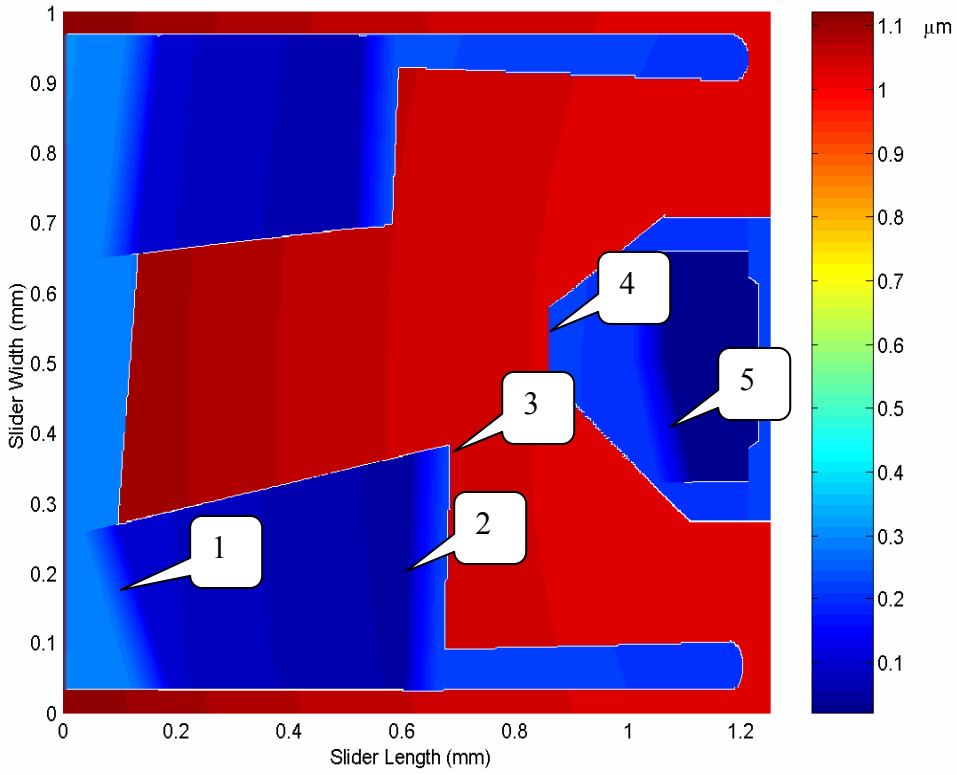

Figure 8, Locations for comparing different forces by 2-D and 3-D modeling

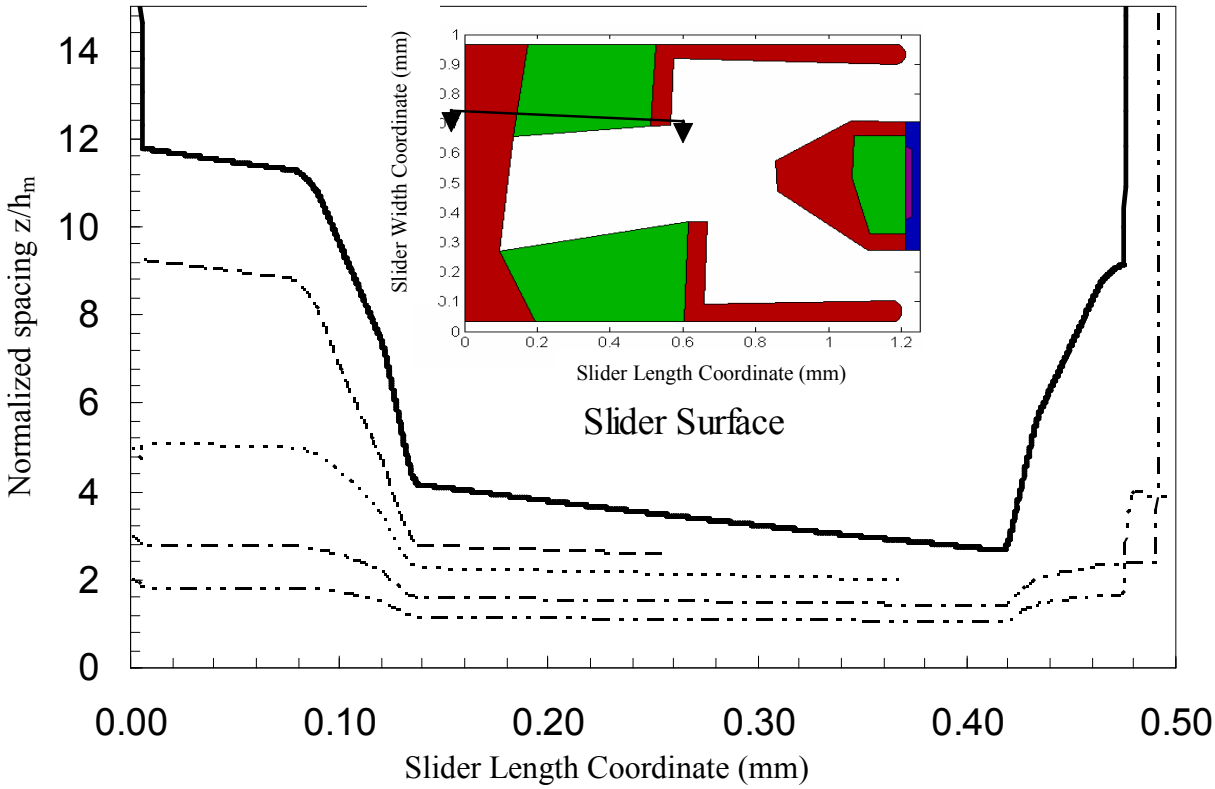

Figure 9, Particle flying paths at various starting positions.

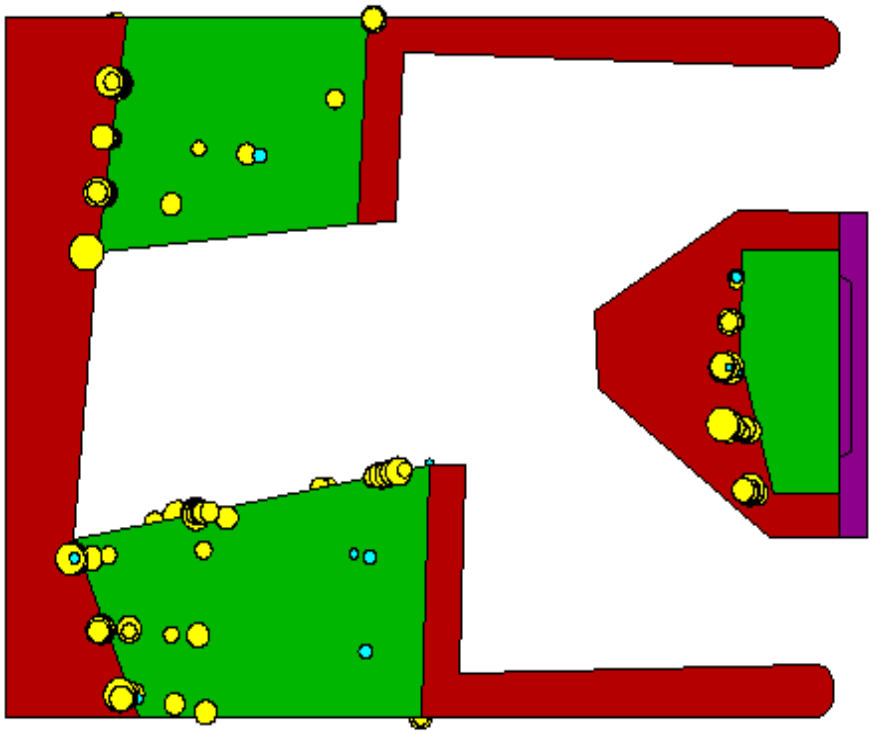

(a) w/o transverse flow

(b) with transverse flow

Figure 10, Comparison between particle contamination profiles using analysis without and with transverse flow effects.

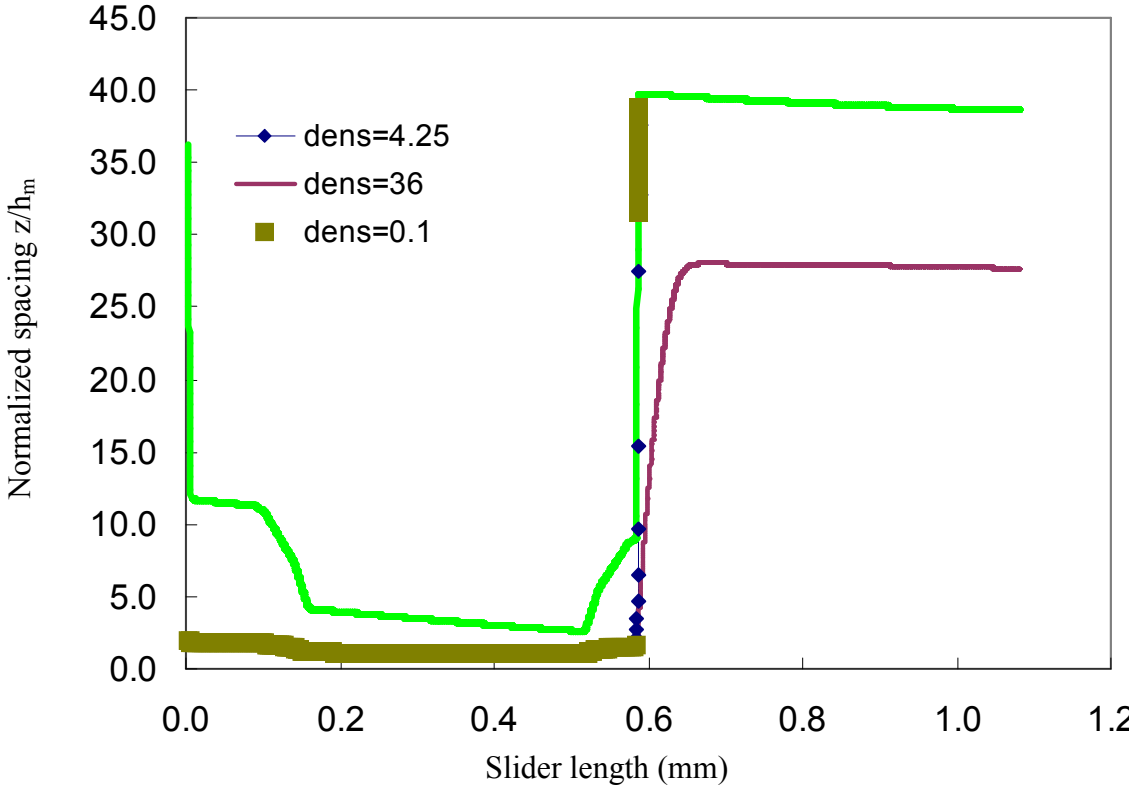

Figure 11, Particle contamination regions for different densities.

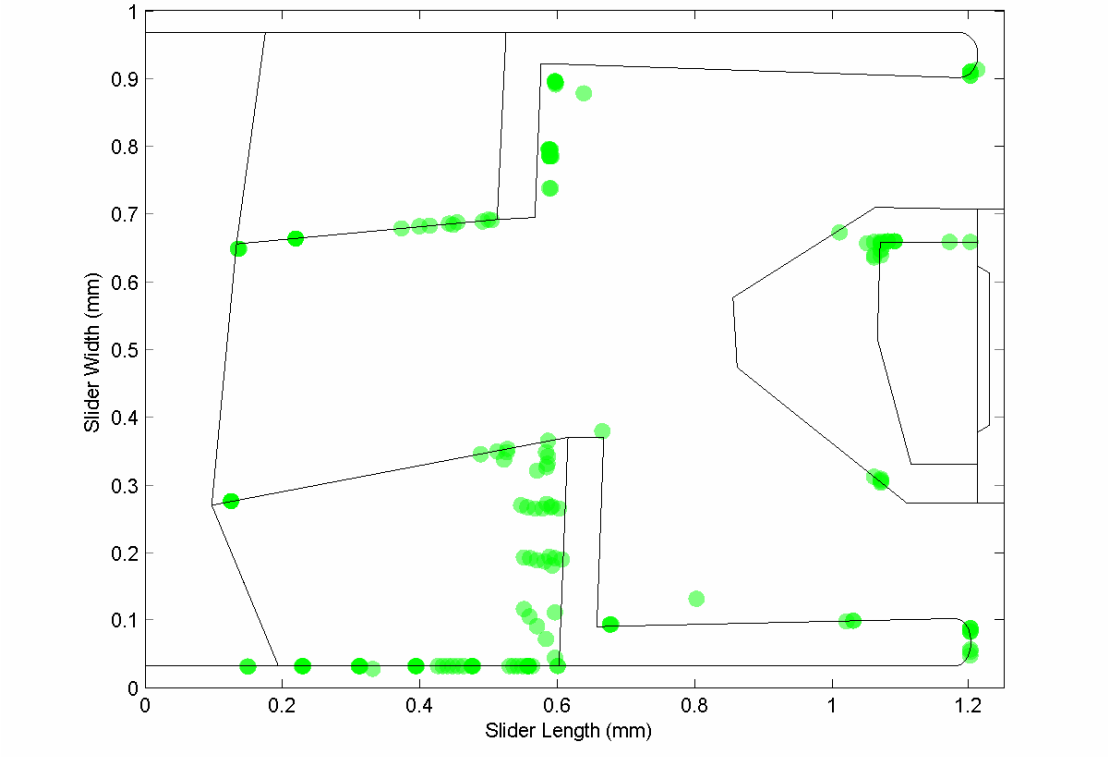

(a) Particle density: 4.5 g/cm^3

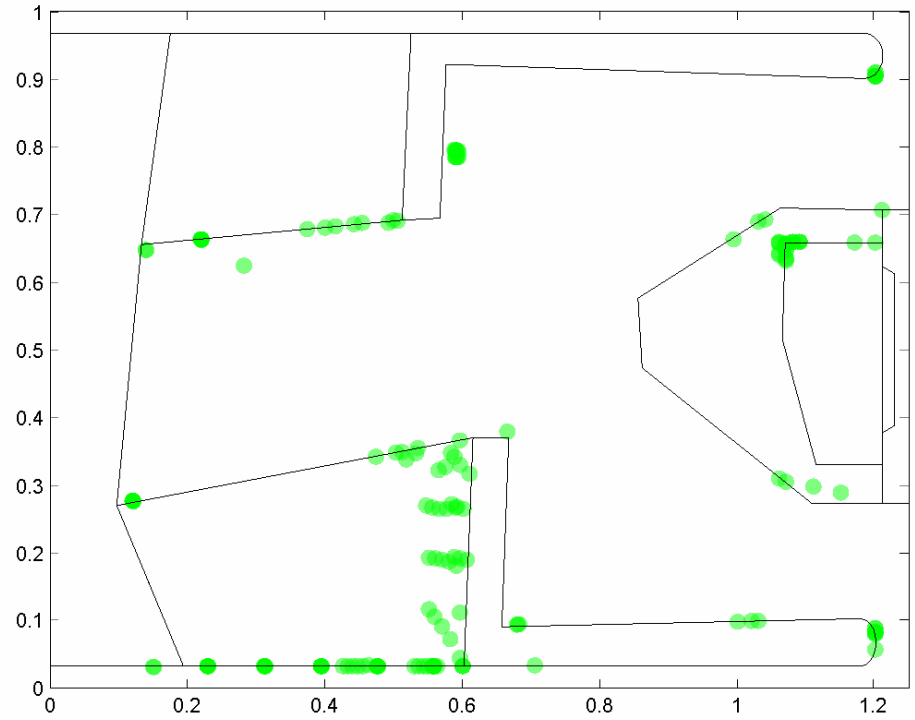

(b) Particle density: 7.8 g/cm^3

Figure 12, Comparison between particle contamination profiles with different densities

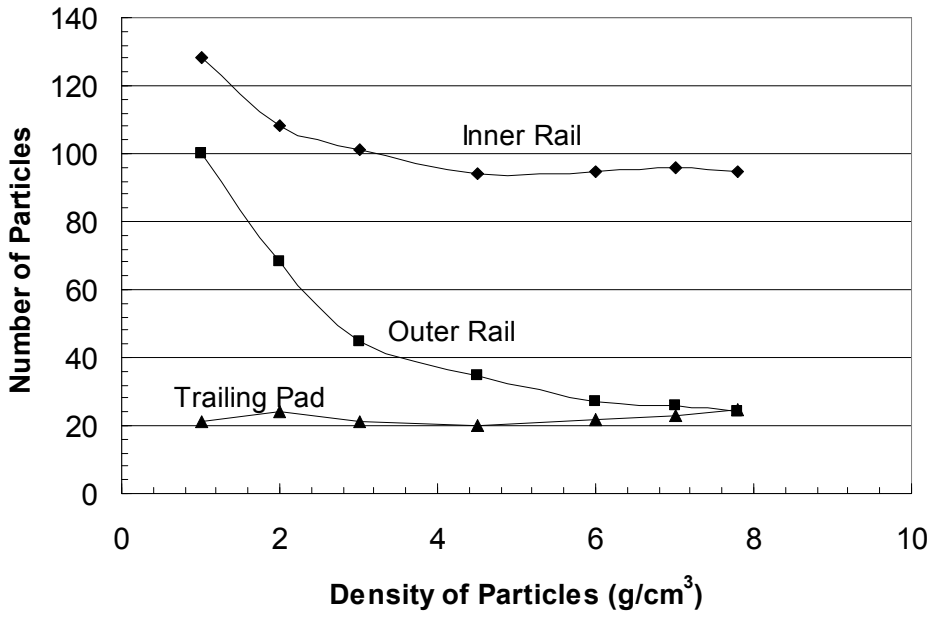

Figure 13, Particle contamination static characteristics for the slider air-bearing.

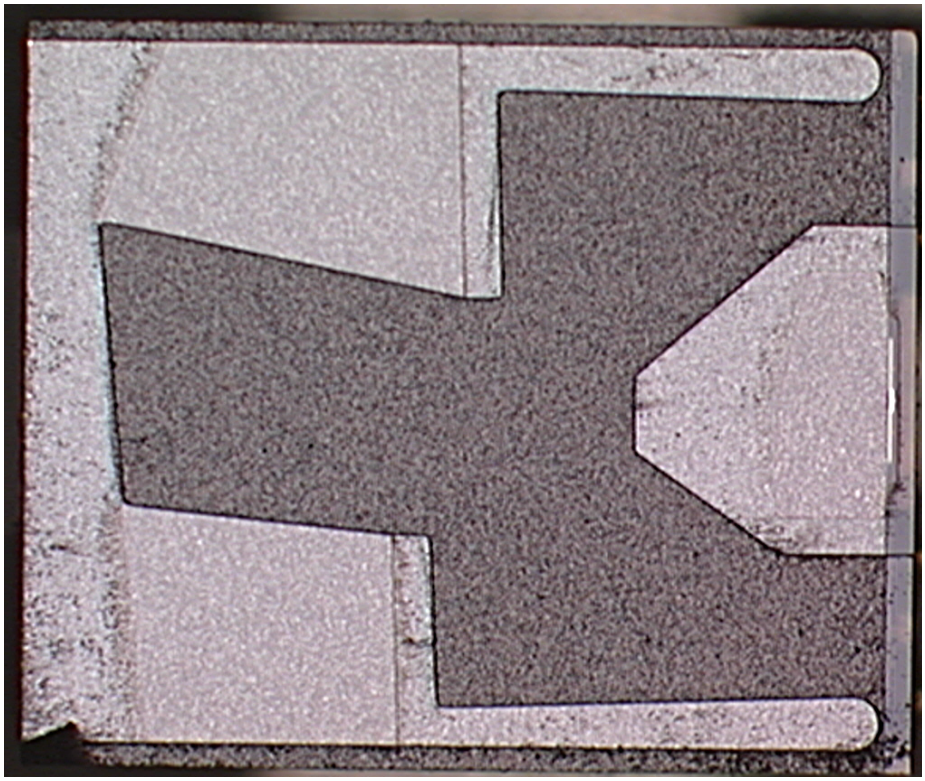

Figure 14, Experimental observed particle contamination profile on the slider

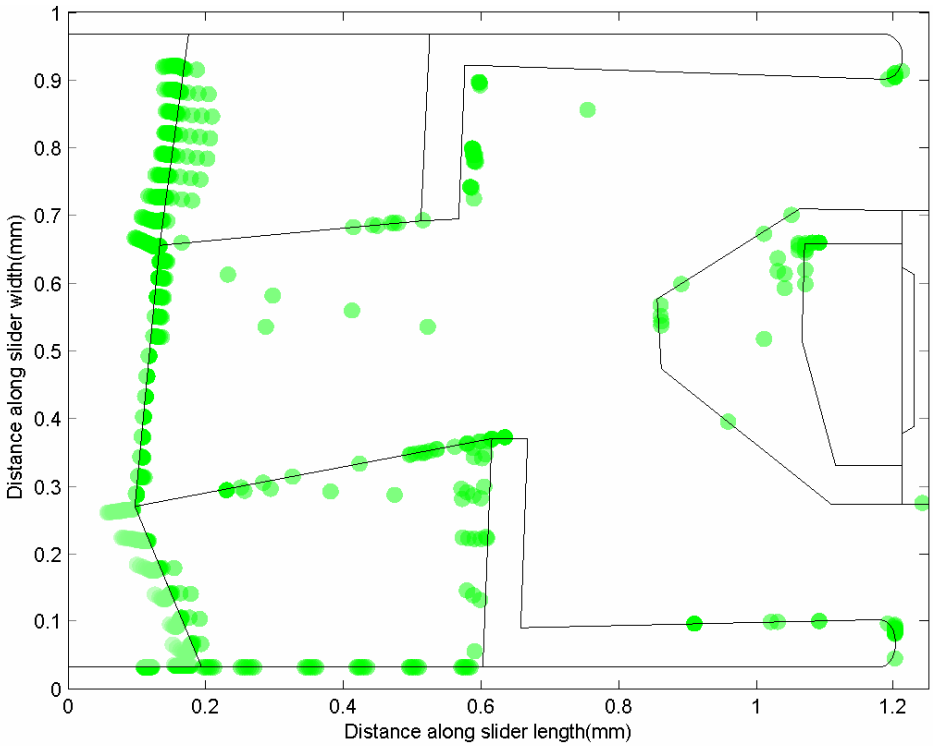

Figure 15, Numerical simulated particle contamination profile for the same slider

Table 1 Comparison between Different Forces by2-D and 3-D Modeling

	Drag Force (Micro Newton)		Saffmann Lift Force (Micro Newton)	
	2-D	3-D	2-D	3-D
1	-0.1E-11	-0.5E-9	0.3E-11	0.5E-11
2	0.14E-10	0.4E-8	0.14E-10	0.2E-9
3	0.1E-9	0.16E-7	0.25E-9	0.2E-10
4	-0.2E-9	-0.1E-6	0.1E-9	0.7E-10
5	-0.4E-10	-0.2E-9	0.14E-10	0.15E-10